

Majorana Zero Modes Emulated in a Magnetic Molecule Chain

Silas Hoffman,¹ Jie-Xiang Yu,¹ Shuang-Long Liu,¹ ChristiAnna Brantley,² Gautam D. Stroschio,³ Ryan G. Hadt,³ George Christou,² Xiao-Guang Zhang,¹ and Hai-Ping Cheng^{1,*}

¹*Department of Physics, Center for Molecular Magnetic Quantum Materials and Quantum Theory Project, University of Florida, Gainesville, Florida 32611, USA*

²*Department of Chemistry and Center for Molecular Magnetic Quantum Materials, University of Florida, Gainesville, Florida 32611, USA*

³*Division of Chemistry and Chemical Engineering, Arthur Amos Noyes Laboratory of Chemical Physics, California Institute of Technology, Pasadena, California 91125, USA*

We propose molecular magnets as a platform to emulate Majorana zero modes (MZMs). Using a quantum chemistry approach, we identify several candidates and predict a Co trimer to have sufficient properties to host MZMs. Parameters of the quantum spin Hamiltonian describing the three coupled magnetic centers are extracted from ab initio calculations. The low-energy subspace of this material realizes an effective anisotropic spin-1/2 chain. We show the presence of MZMs in this system and find that their response to electronic paramagnetic resonance provides an experimentally realizable signature.

Majorana zero modes (MZMs) are persistent exotic states localized to the ends of one-dimensional topological superconductors, and have garnered a particular interest owing to their non-Abelian exchange statistics [1] and potential application for quantum computing [2, 3]. Theoretical models that realize topological superconductivity by constructing heterostructures of conventional materials, such as semiconducting quantum wires and *s*-wave superconductors [4–6], have launched a fervent experimental search to find MZMs. While the appeal to realize topological superconductivity using conventional materials is attractive, their complicated synthesis and measurement [7–11] can lead to false positives in the identification of MZMs [12–15].

Rather than realizing MZMs in electronic systems, several proposals have suggested emulation of MZMs [16] by exploiting the mapping [17] between a spin-1/2 Ising chain and a spinless one-dimensional topological superconductor supporting localized MZMs [18]. In contrast to semiconductor-based MZMs, the nonlocal transformation which fermionizes the spins also destroys their topological protection. Nonetheless, recent experimental results suggest that MZMs emulated in photonic systems [19] and on quantum computers [20] retain their unconventional exchange statistics. While these experimental achievements have shown an impressive control of quantum systems, perhaps a more natural environment to realize MZMs is directly in a quantum spin chain [21, 22]. Moreover, in quantum spin chains, several exotic properties of electronic MZMs, such as perfect Andreev reflection [23], fractional Josephson current [24], and non-Abelian braiding statistics [25], have a corresponding spin analogue.

Using spin chains as a platform for MZMs faces difficult challenges. On the one hand, the coupling between moments on the chain must be sufficiently strong and anisotropic to ensure an ordered ground state and

a gapped bulk spin excitation. On the other hand, weak coupling and low-dimensionality cause disorder, which is detrimental to both the existence of the MZMs and their effective detection. Consequently, neither a concrete experimental realization nor a theoretically proposed material has been suggested to emulate MZMs using a quantum spin chain. These difficulties can be bypassed using magnetic molecules and exploiting the accrued expertise of their field of study. The power of using molecular magnets is in (1) the vast freedom in tuning magnetic anisotropy and inter-metal ion exchange by local chemical environment and by ligands, (2) monodispersive nature assuring low disorder, and (3) ab initio techniques which can quantitatively predict the expected experimental parameters [26–28]

In this letter, we suggest one such viable molecular magnet example: $\text{Co}_3(\text{SALPN})_2(\text{O}_2\text{CCH}_3)_2 \cdot (\text{OCHNH}_2)_2$. Using first-principles density functional theory (DFT) [29, 30], we build a quantum spin model for this candidate. Projecting onto a low-energy subspace of states, we realize a rich effective Hamiltonian which, for a sufficiently small external magnetic field, supports the emulation of MZMs. By simulating an electron paramagnetic resonance (EPR) spectroscopy measurement, we find that the effective occupancy of the MZMs can be extracted and we predict the expected experimental EPR signatures of this material.

DFT calculations.— To keep the calculations simple in the search for viable spin chain candidates, we study molecular magnets with three metal centers, which are the smallest molecule chains that can host MZMs. Having studied several candidate materials with sizable anisotropy [31], we focus on the Co trimer $\text{Co}_3(\text{SALPN})_2(\text{O}_2\text{CCH}_3)_2 \cdot (\text{OCHNH}_2)_2$ which has been experimentally synthesized with a different solvent [32]. Fig. 1(a) shows the atomic structure of the Co trimer.

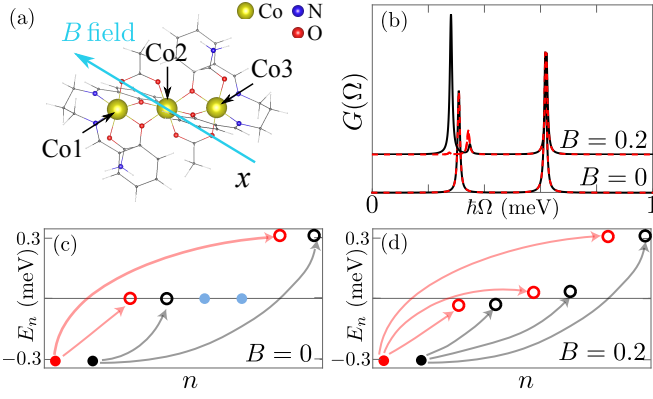


Figure 1. (a) Atomic structure of a single Co₃ molecule with OCHNH₂ solvent molecules in a dc magnetic field B applied perpendicular to the magnetic easy axes of Co atoms. (b) EPR signal as a function of ac-applied magnetic field frequency Ω . The solid (black) and dashed (red) line are the response of the two ground degenerate states. The spectra are plotted for $B = 0$ (c) and $B = 0.2$ (d) where ac-magnetic-field-induced transitions between the ground states (filled red circles and black circles) and the accessible excited states (open red and black circles) are indicated by arrows; inaccessible excited states are marked by filled blue circles.

The three Co atoms from left to right are labeled as Co1, Co2, and Co3, respectively. Each Co atom has a local spin of $S = 3/2$ corresponding to the +2 oxidation state.

This molecule is well-described by a spin Hamiltonian, $\hat{H} = \hat{H}_{\text{ex}} + \hat{H}_a + \hat{H}_r$, with an isotropic exchange interaction, $\hat{H}_{\text{ex}} = J \sum_{i=1}^2 \hat{\mathbf{S}}_i \cdot \hat{\mathbf{S}}_{i+1}$, and an on-site axial and rhombic anisotropy,

$$\hat{H}_a = \sum_{i=1}^3 [D_i (\hat{\mathbf{S}}_i \cdot \mathbf{z}_i)^2], \quad (1)$$

and

$$\hat{H}_r = \sum_{i=1}^3 E_i [(\hat{\mathbf{S}}_i \cdot \mathbf{x}_i)^2 - (\hat{\mathbf{S}}_i \cdot \mathbf{y}_i)^2], \quad (2)$$

respectively. J is the exchange coupling constant between two nearest-neighbor Co atoms and D_i and E_i are local axial and rhombic zero field splitting parameters for the i th Co atom. The axes of anisotropy for each Co atom are, in general, noncollinear and therefore we express the anisotropy Hamiltonian in the local frame defined by unit vectors \mathbf{x}_i , \mathbf{y}_i and \mathbf{z}_i . Because of the inversion symmetry of this complex, the exchange coupling is constant and the on-site anisotropies of Co1 and Co3 are equal, i.e. $D_1 = D_3$ and $E_1 = E_3$.

DFT calculations are carried out using the Vienna Ab initio Simulation Package [33, 34] with an energy cutoff of 600 eV for plane waves, the projector augmented wave pseudopotentials [35, 36] and the Perdew-Burke-Ernzerhof (PBE) exchange-correlation

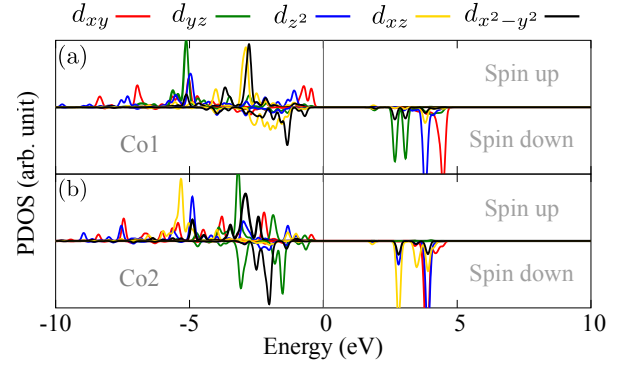


Figure 2. PDOS of the Co₃ molecule with OCHNH₂ solvent molecules. The panel (a) is for Co1 at the end of the Co chain and (b) for Co2 in the middle. The Fermi level is set to zero.

energy functional [37]. The energy and force tolerances are set to 10^{-8} eV and 0.001 eV/Å respectively. We fix the magnetic core including Co, O and N atoms to the experimental structure and impose inversion symmetry during structural relaxation. We apply the DFT+ U method [38] and set the on-site Coulomb and exchange parameters to be 5.0 and 0.9 eV respectively for Co 3d electrons to account for strong correlation effects. We extract J using the broken-symmetry method [28, 29] based on DFT total energies without spin-orbit coupling (SOC). Anisotropy parameters D_i and E_i are extracted by treating spins as classical quantities based on DFT total energies with SOC, which is included self-consistently with constraint on the direction of local spins. [41] The fitted values are $J = -0.092$ meV, $D_1 = D_3 = -0.668$ meV, $D_2 = -0.522$ meV, $E_1 = E_3 = -0.069$ meV, $E_2 = -0.033$ meV. The negative J signifies ferromagnetic coupling between Co1 (or Co3) and Co2. The negative D_i values indicate that each Co atom has a magnetic easy axis. The direction of magnetic easy axis is $(\theta = 42.9^\circ, \phi = 102.4^\circ)$ for Co1 (or Co3) and $(\theta = 26.5^\circ, \phi = 177.8^\circ)$ for Co2. The difference in the local magnetic anisotropy between Co1 (or Co3) and Co2 originates from the different chemical environment. Co1 (or Co3) is bonded with four oxygen atoms and two nitrogen atoms while Co2 is bonded with six oxygen atoms. As a result, d orbitals are split and occupied differently as shown by the projected density of states (PDOS) in Fig. 2. The ratio D_i/J is 7.3 for Co1 (or Co3) and 5.7 for Co2.

Effective Hamiltonian.— While MZMs are known to be realized in an Ising chain [31], the model Hamiltonian used in the DFT calculation is considerably more complicated. Nonetheless, because the exchange interaction and rhombic anisotropy are small compared to the axial anisotropy, we can project onto a subspace of states. Our low energy basis is spanned by the eigenstates of $\hat{H}_a + \hat{H}_B$ where the first term is defined by Eq. (1) and $\hat{H}_B = -B \sum_{i=1}^3 \mathbf{S}_i \cdot (\mathbf{z}_1 \times \mathbf{z}_2)$ describes an applied

magnetic field simultaneously perpendicular to the easy axes of the Co atoms. We label the low energy eigenstates of each Co site by $|\uparrow\rangle$ and $|\downarrow\rangle$, respectively. Each site effectively furnishes two states, analogous to the spin-1/2 chain, and the tensor product of these states furnish a low energy basis.

Projecting $\hat{H} + \hat{H}_B$ onto the low energy states, we find the effective Hamiltonian takes the form,

$$\hat{H}^{\text{eff}} = - \sum_{i=1}^2 [J^x \sigma_i^x \sigma_{i+1}^x + J^y \sigma_i^y \sigma_{i+1}^y + J^z \sigma_i^z \sigma_{i+1}^z + \mathcal{D}(\sigma_i^x \sigma_{i+1}^y - \sigma_i^y \sigma_{i+1}^x)] - \sum_{i=1}^3 \mu_i \sigma_i^z, \quad (3)$$

where the Pauli matrices act on the low energy basis of the i th Co. Eq. (3) is a spin-1/2 Heisenberg XYZ model with a Dzyaloshinskii-Moriya interaction (DMI) and site-dependent magnetic field. The spin-1/2 Hamiltonian inherits the on-site anisotropy of the spin-3/2 model as an anisotropy in the exchange interaction, i.e. $J_x \neq J_y \neq J_z$ in general. The noncollinearity of the axes of anisotropy is expressed as a renormalization of the exchange interaction parameters as well as a Dzyaloshinskii-Moriya interaction. This broken inversion symmetry, although not present in the original spin-3/2 Hamiltonian, is necessary to capture the effect of noncollinear anisotropy which will manifest in the EPR spectra below.

The parameters have an implicit, albeit convoluted, dependence on the magnetic field and we have dropped a magnetic-field-dependent constant energy. When the magnetic field is small compared to the axial anisotropy, $b = B/D \ll 1$, the parameters entering Eq. (3) are polynomial in b ,

$$\begin{aligned} J^x &= JS^2(1 - b^2/4 - Sb^4/16) \cos \theta, \\ J^y &= (JS^4b^4/16) \cos \theta, \quad J^z = JS^4b^4/16, \\ \mathcal{D} &= J(b^2/16 - S^2b^4/16) \sin \theta, \\ \mu_1 &= \mu_3 = S(bE - b^3[4(1+E) + 9J])/32, \\ \mu_2 &= S(bE - b^3[2(1+E) + 9J])/16, \end{aligned} \quad (4)$$

where, for simplicity, we have considered $D_1 = D_2 = D_3 = D$ and $E_1 = E_2 = E$. θ is the angle between the easy axes, i.e. $\mathbf{z}_1 \cdot \mathbf{z}_2 = \cos \theta$.

When $B = 0$, Eq. (3) is a spin-1/2 Ising model wherein the MZMs are written as $\gamma = \sigma_1^x$ and $\gamma' = \sigma_1^z \sigma_2^z \sigma_3^y$ [31]. Plotting the parameters in Eq. (3) for homogeneous exchange and anisotropy and similar J/D and E/D ratios to those obtained in the DFT calculation [Fig. 3(a)], we find that the Ising exchange largely dominates over the exchange interaction and DMI. Accordingly, we estimate the topological phase transition to be roughly when $\mu_2 \simeq J^x$, corresponding to $B \approx D$. That is, for an infinite chain, MZMs remain exponentially localized to the ends of the chain when $B < D$ and vanish

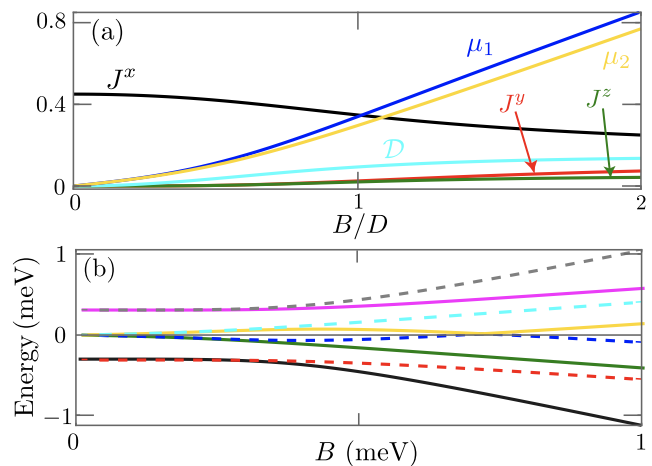


Figure 3. (a) Values of effective parameters in Eq. (3), in units of $D_1 = D_2 = D_3 = D$, obtained by projecting the trimer Hamiltonian with $J = 0.2D$ and $E_1 = E_2 = 0.1D$ and $\theta = 0$. (b) Spectrum of Eq. (3) as a function of applied magnetic field, B , approximately along the $(\theta, \phi) \approx (\pi/3, -\pi/10)$, such that it is perpendicular to the axes of anisotropy of the Co's, using the parameters found using DFT.

when $B > D$. Employing the methodology outlined in Ref. [42], one can find an explicit expression for the MZMs at finite B dressed according to the additional interactions in Eq. (3).

With the effective Hamiltonian prepared, upon allowing for inhomogeneous axial and rhombic anisotropy, we proceed to calculate the spectrum using the values obtained from DFT [Fig. 3(b)]. The presence of MZMs is reflected in the double degeneracy of the states. When $B = 0$, the system is simply an Ising chain and the lowest doublet of states correspond to fully spin polarized states, $|\uparrow\uparrow\uparrow\rangle$ and $|\downarrow\downarrow\downarrow\rangle$. The four states at zero energy are those states with single spin flip at the end of the chain, $|\downarrow\uparrow\uparrow\rangle$, $|\uparrow\uparrow\downarrow\rangle$, $|\uparrow\downarrow\uparrow\rangle$, and $|\downarrow\downarrow\uparrow\rangle$. The highest energy correspond to the middle spin being flipped, $|\uparrow\downarrow\uparrow\rangle$ and $|\downarrow\uparrow\downarrow\rangle$. As the magnetic field is turned on, these states mix according to the effective Hamiltonian. The MZMs overlap and begin to hybridize when $B \approx 0.3D$, breaking the double degeneracy. This dependence of the spectrum on the magnetic field can be used as a signature that MZMs are present in the trimer.

Spectral analysis.— To probe the spectrum, we calculate the response of a ground state to a transverse ac-magnetic field, i.e. simulate EPR. The ac-magnetic field within the spin-3/2 model is $\hat{H}_{\text{EPR}}(t) = h_{\text{ac}} \cos(\Omega t) \sum_{i=1}^3 \mathbf{S}_i \cdot (\mathbf{z}_1 \times \mathbf{z}_2)$ which maps to $\hat{H}_{\text{EPR}}^{\text{eff}}(t) = \cos(\Omega t) \sum_{i=1}^3 h_{i,\text{ac}}^{\text{eff}} \sigma_i^z$ with $h_{i,\text{ac}}^{\text{eff}} = SB/4D_i$ in the effective spin-1/2 model. The linear response of the system to the

ac field is [30, 31]

$$G(\Omega) \sim \int dt \cos(\Omega t) \left\langle \left\{ \sum_{i=1}^N h_{i,\text{ac}}^{\text{eff}} \sigma_i^z, \sum_{j=1}^N h_{j,\text{ac}}^{\text{eff}} \sigma_j^z(t) \right\} \right\rangle, \quad (5)$$

where the expectation is with respect to one of the ground states and $\sigma_j^z(t)$ evolves according to Eq. (3). The form of the ac-magnetic field implies that the resultant EPR signal measures transitions between states that differ by one spin flip; this statement is exact in the case when $B = 0$ and can be used to guide our intuition for finite magnetic field.

When $B = 0$, the EPR signal [Fig. 1(b)] is identical for the two ground states, i.e. the black solid line and red dashed line overlap. This is a consequence of the double degeneracy of the ground states and excited states [Fig. 1(c)]. Focusing on the positive spin ground state, indicated by the red dot in Fig. 1(c), the peak at $\Omega \approx 0.3$ corresponds to the transition between $|\uparrow\uparrow\uparrow\rangle$ and $(|\downarrow\uparrow\uparrow\rangle + |\uparrow\uparrow\downarrow\rangle)/\sqrt{2}$ and the peak at $\Omega \approx 0.6$ corresponds to the transition between $|\uparrow\uparrow\uparrow\rangle$ and $|\uparrow\downarrow\uparrow\rangle$. We note that the state $(|\downarrow\uparrow\uparrow\rangle - |\uparrow\uparrow\downarrow\rangle)/\sqrt{2}$ is inaccessible because it is inversion asymmetric. Reversing the spin direction, one obtains the transitions between the other ground state, $|\downarrow\downarrow\downarrow\rangle$, and the analogous excited states, highlighted in black and grey in Fig. 1(c).

When $B = 0.2$, the spectrum [Fig. 1(d)] shows a splitting of the four states at zero energy to two pairs of doublets while the highest and lowest energy states remain degenerate. While difficult to discern in the spectrum, the near zero energy are not degenerate, i.e. $E_3 \neq E_4$ and $E_5 \neq E_6$. Moreover, because the effective inversion symmetry is broken in a finite magnetic field, i.e. $\mathcal{D} \neq 0$, the ac-magnetic field induces transitions between one of the ground states and half of the excited states. As a result, the EPR signal displays five peaks [Fig. 1(b)].

In Fig. 4, we plot the EPR spectrum as a function of Ω and B by summing the EPR intensities from both of the ground states. Here, we have plotted the logarithm of the intensity in order to highlight the fainter features. Should the molecules be probed in thermal equilibrium at temperatures much smaller than the exchange interaction, we expect to observe a spectral dependence on the magnetic field as seen in Fig. 4.

Discussion.— Despite having a deceptively simple starting point of a spin-3/2 Hamiltonian with a homogeneous exchange interaction and on-site anisotropy, the effective spin-1/2 Hamiltonian realizes an anisotropic exchange and breaks inversion symmetry. This points to advantages of molecular magnetic materials as candidates for designer effective Hamiltonians. The machinery and methodology in this work can be used as a blueprint to survey molecular magnetic systems to realize a variety of interesting, effective Hamiltonians which support interactions that

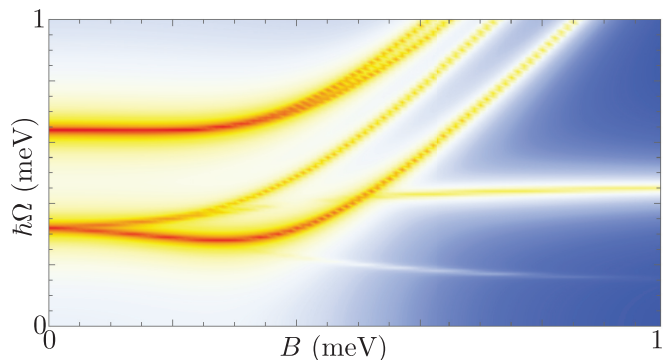


Figure 4. EPR spectrum as a function of ac-magnetic field frequency, Ω , and magnitude of dc-applied magnetic field, B , approximately along the $(\theta, \phi) \approx (\pi/3, -\pi/10)$, such that it is perpendicular to the axes of anisotropy of the Co's, using the parameters found using DFT. Here, we have plotted the logarithm of the intensity to emphasize the presence of smaller peaks.

would be a priori unexpected. For instance, this analysis can be applied to material searches for inhomogeneous Ising chains, inhomogeneous spin ladders, or Kitaev lattices, all of which support Majorana modes at their ends or edges, respectively. Moreover, upon considering a broader class of materials, we expect such an analysis could aid in material searches for emulation of other systems such as quantum spin glasses or strongly correlated quantum systems for use in error mitigation.

Although we merely studied this system theoretically, this molecule with a different solvent has been recently synthesized and EPR spectroscopy is currently being performed which will be included in future publications. Owing to the relative simplicity of the system, as compared with for instance solid state proposals, and the power of ab initio calculations, we expect a positive correlation between our predicted EPR and that observed experimentally.

Acknowledgements.— This work was supported as part of the Center for Molecular Magnetic Quantum Materials, an Energy Frontier Research Center funded by the U.S. Department of Energy, Office of Science, Basic Energy Sciences under Award No. DE-SC0019330. Computations were done using the utilities of National Energy Research Scientific Computing Center, and University of Florida Research Computing systems.

* Correspond to: hping@ufl.edu

- [1] D. A. Ivanov, *Phys. Rev. Lett.* **86**, 268 (2001).
- [2] C. Nayak, S. H. Simon, A. Stern, M. Freedman, and S. Das Sarma, *Rev. Mod. Phys.* **80**, 1083 (2008).
- [3] R. Aguado and L. P. Kouwenhoven, *Physics Today* **73**, 45 (2020).
- [4] R. M. Lutchyn, J. D. Sau, and S. Das Sarma, *Phys. Rev.*

- Lett.* **105**, 077001 (2010).
- [5] Y. Oreg, G. Refael, and F. von Oppen, *Phys. Rev. Lett.* **105**, 177002 (2010).
- [6] J. Alicea, *Phys. Rev. B* **81**, 125318 (2010).
- [7] V. Mourik, K. Zuo, S. M. Frolov, S. R. Plissard, E. P. A. M. Bakkers, and L. P. Kouwenhoven, *Science* **336**, 1003 (2012).
- [8] M. T. Deng, C. L. Yu, G. Y. Huang, M. Larsson, P. Caroff, and H. Q. Xu, *Nano Letters* **12**, 6414 (2012).
- [9] A. Das, Y. Ronen, Y. Most, Y. Oreg, M. Heiblum, and H. Shtrikman, *Nature Physics* **8**, 887 (2012).
- [10] H. O. H. Churchill, V. Fatemi, K. Grove-Rasmussen, M. T. Deng, P. Caroff, H. Q. Xu, and C. M. Marcus, *Phys. Rev. B* **87**, 241401 (2013).
- [11] S. M. Albrecht, A. P. Higginbotham, M. Madsen, F. Kuemmeth, T. S. Jespersen, J. Nygård, P. Krogstrup, and C. M. Marcus, *Nature* **531**, 206 (2016).
- [12] C.-X. Liu, J. D. Sau, T. D. Stanescu, and S. Das Sarma, *Phys. Rev. B* **96**, 075161 (2017).
- [13] C. Reeg, O. Dmytruk, D. Chevallier, D. Loss, and J. Klinovaja, *Phys. Rev. B* **98**, 245407 (2018).
- [14] E. Prada, P. San-Jose, M. W. A. de Moor, A. Geresdi, E. J. H. Lee, J. Klinovaja, D. Loss, J. Nygard, R. Aguado, and L. P. Kouwenhoven, *Nature Reviews Physics* **2**, 575 (2020).
- [15] P. Yu, J. Chen, M. Gomanko, G. Badawy, E. P. A. M. Bakkers, K. Zuo, V. Mourik, and S. M. Frolov, *Nature Physics* **17**, 482 (2021).
- [16] L. Jiang, T. Kitagawa, J. Alicea, A. R. Akhmerov, D. Pekker, G. Refael, J. I. Cirac, E. Demler, M. D. Lukin, and P. Zoller, *Phys. Rev. Lett.* **106**, 220402 (2011).
- [17] E. Lieb, T. Schultz, and D. Mattis, *Ann. Phys.* **16**, 407 (1961).
- [18] A. Y. Kitaev, *Physics-Uspekhi* **44**, 131 (2001).
- [19] J.-S. Xu, K. Sun, Y.-J. Han, C.-F. Li, J. K. Pachos, and G.-C. Guo, *Nature Communications* **7**, 13194 (2016).
- [20] J. P. T. Stenger, N. T. Bronn, D. J. Egger, and D. Pekker, *Phys. Rev. Research* **3**, 033171 (2021).
- [21] Y. Tserkovnyak and D. Loss, *Phys. Rev. A* **84**, 032333 (2011).
- [22] F. L. Pedrocchi, S. Chesi, S. Gangadharaiah, and D. Loss, *Phys. Rev. B* **86**, 205412 (2012).
- [23] S. Hoffman, D. Loss, and Y. Tserkovnyak, arXiv preprint arXiv:1810.11470 (2018).
- [24] P.-X. Shen, S. Hoffman, and M. Trif, *Phys. Rev. Research* **3**, 013003 (2021).
- [25] S. Backens, A. Shnirman, Y. Makhlin, Y. Gefen, J. E. Mooij, and G. Schön, *Phys. Rev. B* **96**, 195402 (2017).
- [26] A. E. Thuijs, X. G. Li, Y. P. Wang, K. A. Abboud, X. G. Zhang, H. P. Cheng, and G. Christou, *Nature Communications* **8**, 500 (2017).
- [27] T. Ghosh, J. Marbey, W. Wernsdorfer, S. Hill, K. A. Abboud, and G. Christou, *Physical Chemistry Chemical Physics* **23**, 8854 (2021).
- [28] J. X. Yu, G. Christou, and H. P. Cheng, *Journal of Physical Chemistry C* **124**, 14768 (2020).
- [29] P. Hohenberg and W. Kohn, *Physical Review* **136**, B864 (1964).
- [30] W. Kohn and L. J. Sham, *Physical Review* **140**, A1133 (1965).
- [31] See Supplemental Material which includes the results of quantum chemistry calculations of monomers, the results of DFT calculations of additional molecular chains, and an EPR analysis of the spin-1/2 Ising chain.
- [32] A. Gerli, K. S. Hagen, and L. G. Marzilli, *Inorganic Chemistry* **30**, 4673 (1991).
- [33] G. Kresse and J. Furthmüller, *Computation Materials Science* **6**, 15 (1996).
- [34] G. Kresse and J. Furthmüller, *Physical Review B* **54**, 11169 (1996).
- [35] P. E. Blöchl, *Physical Review B* **50**, 17953 (1994).
- [36] G. Kresse and D. Joubert, *Physical Review B* **59**, 1758 (1999).
- [37] J. P. Perdew, K. Burke, and M. Ernzerhof, *Physical Review Letters* **77**, 3865 (1996).
- [38] A. I. Liechtenstein, V. I. Anisimov, and J. Zaanen, *Physical Review B* **52**, R5467 (1995).
- [28] E. Ruiz, J. Cano, S. Alvarez, and P. Alemany, *Journal of Computational Chemistry* **20**, 1391 (1999).
- [29] E. Ruiz, A. Rodríguez-Forteza, J. Cano, S. Alvarez, and P. Alemany, *Journal of Computational Chemistry* **24**, 982 (2003).
- [41] P. Liu, S. Khmelevskiy, B. Kim, M. Marsman, D. Li, X.-Q. Chen, D. D. Sarma, G. Kresse, and C. Franchini, *Physical Review B* **92**, 054428 (2015).
- [42] A. Alexandradinata, N. Regnault, C. Fang, M. J. Gilbert, and B. A. Bernevig, *Phys. Rev. B* **94**, 125103 (2016).
- [30] G. O. Berim and A. R. Kessel, *Physica B+C* **96**, 71 (1979).
- [31] R. Kubo and K. Tomita, *Journal of the Physical Society of Japan* **9**, 888 (1954).

Supplemental Material for “Majorana Zero Modes Emulated in a Magnetic Molecule Chain”

Silas Hoffman¹, Jie-Xiang Yu¹, Shuang-Long Liu¹, ChristiAnna Brantley², Guatam D. Stroschio³, Ryan G. Hadt³, George Christou², Xiao-Guang Zhang¹, and Hai-Ping Cheng¹

¹ *Department of Physics, Center for Molecular Magnetic Quantum Materials and Quantum Theory Project, University of Florida, Gainesville, Florida 32611, USA*

² *Department of Chemistry and Center for Molecular Magnetic Quantum Materials, University of Florida, Gainesville, Florida 32611, USA*

³ *Division of Chemistry and Chemical Engineering, Arthur Amos Noyes Laboratory of Chemical Physics, California Institute of Technology, Pasadena, California 91125, USA*

I. QUANTUM CHEMISTRY CALCULATIONS OF MONOMERS

We examined a few monomers that may be candidate systems of longer chains for future synthesis. The results are tabulated in Table I.

Material	D (cm ⁻¹)			E/D		
	CASSCF	NEVPT2	Experiment	CASSCF	NEVPT2	Experiment
Plass Monomers [1]						
2-Co1	-134.6	-106.6		0.08	0.08	
2-Co2	-133.4	-109.5		0.11	0.11	
3-Co1	-128.2	-109.0		0.15	0.14	
3-Co2	-177.8	-179.9		0.14	0.12	
Co(II) Monomers						
[Co(II)](SPh ₄) ²⁻	-85.2		-70.0 [2]	0.00		0.09
Co(II) Schiff base, cn=5	-33.4		-38.9 [3]	0.25		
Ni(II) Monomers						
*[Ni(II)(iz) ₄ (ac) ₂] ²⁺	46.7		-22.3 [4]	0.28		

Table I. D and E are the axial and rhombic zero field splitting (ZfS) parameters respectively. CASSCF/NEVPT2 calculations are performed using minimal active space of $3d$ orbitals.* $3d$ orbitals are included in active space (8e,5o).

Our calculations were performed using ORCA version 4.2.1.[5, 6] N-electron valence state second-order perturbation theory (NEVPT2) corrected complete active space self-consistent field (CASSCF) single point calculations [7–9] were performed on all Plass monomers. [1] Because of the agreement between CASSCF and NEVPT2 values for D and E/D , only CASSCF was performed for the other complexes. The DKH-def2-TZVP [10] basis set (relativistic recontraction of def2-TZVP [11]) was used on all atoms. SCF convergence criteria with an energy tolerance of 10^{-7} Hartrees were applied. For cobalt complexes, a minimal active space (7e,5o) consisting of the $3d$ orbitals was used for these calculations ten quartets and forty doublets were included in the state-averaging to account for all the ligand field transitions. For the nickel complex complexes, a minimal active space (8e,5o) consisting of the $3d$ orbitals was used for these calculations ten triplets and fifteen doublets were included in the state-averaging to account for all the ligand field transitions.

For DFT optimization of structures, the BP86 [12–14] DFT functional was used for structural optimizations. Def2-SVP [11] and Split-RI-J [15–20], the default and recommended version of resolution of identities approximation was used; the finest available grids were used (GRID7 NOFINALGRID). Tight SCF convergence criteria, which has a convergence tolerance of 10^{-8} Hartrees, was applied for all DFT calculations. The Plass monomers [1] were optimized using a Zn containing analog to speed SCF convergence similar to as had been done previously. For [Co(II)(SPh₄)]²⁻, a previously published, DFT-optimized structure was used. [21] The Co(II) Schiff base [3] and the [Ni(II)(iz)₄(ac)₂]²⁺ structure [4] were optimized from their crystal structures; in the latter case only hydrogens were optimized.

II. DFT CALCULATIONS OF ADDITIONAL MOLECULAR CHAINS

A few Ising crystal systems are reported for which, truncation of long chains into short chains (say 3–10

metal centers) are desirable. In the following, we present DFT calculation results on three such systems, namely CoCl₂(thiourea)₄ (nickname DTC), CoNa(N₃)₂(L) [22],

and $\text{Co}(\text{NCS})_2(\text{thiourea})_2$ [23].

A. DTC

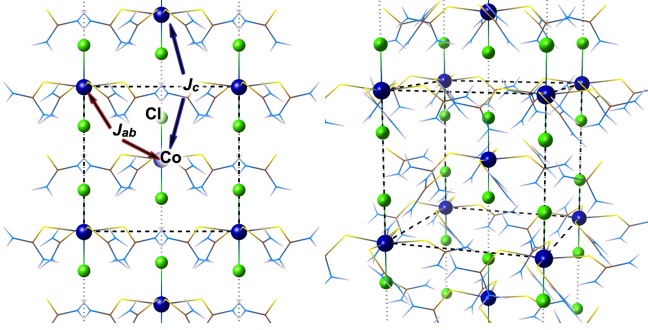


Figure 5. The structure of molecular crystal DTC in the side view and the perspective view. Blue and green balls represent Co and Cl atoms, respectively. The dotted Cl-Cl bonds indicate the Van der Waals interactions. The intra- and inter-chain Co-Co interaction J_c and J_{ab} are labeled.

Molecular magnets $\text{CoCl}_2(\text{thiourea})_4$ (Dichloro-tetrakis(thiourea)-cobalt, DTC, thiourea = $\text{SC}(\text{NH}_2)_2$) is the Co substitution of $\text{NiCl}_2(\text{thiourea})_4$ (Dichloro-tetrakis(thiourea)-nickel, DTN) which is a quasi one-dimensional quantum molecular magnetic material [24–26]. DTC is antiferromagnetic materials with Neel temperature 0.92 K and is suggested to have magnon conductivity below the Neel temperature [27].

The bulk structure of crystalline DTC has a body-centered tetragonal lattice where two DTC molecules are in each tetragonal cell. An $1 \times 1 \times 2$ supercell with the double size along c -axis is used to evaluated the intra- and inter-chain Co-Co interaction labeled in Fig. 5 based on to the total energy results. By using broken-symmetry method [28, 29], we obtained the intra-chain interaction $J_c = 0.18$ meV is ferromagnetic coupling and the inter-chain interaction $J_{ab} = -0.075$ meV is antiferromagnetic coupling. Similar to DTN, the strong intra-chain interaction in DTC, is due to the strong Cl-Cl Van der Waals interactions.

Based on the inter-chain antiferromagnetic state, the lowest energy state, we included SOC and investigated the magnetic anisotropy by calculating the total energies with various spin directions. The results are shown in Fig. 6(a). The state with out-of-plane spin directions, corresponding to $\theta = 0$, $\cos^2 \theta = 1$ has the lowest energy, indicating the easy axis is along c axis. The fitting for $E_0 + k_1 \cos^2 \theta + k_2 \cos^4 \theta$ is $k_1 = -75.6$ meV and $k_2 = 24.2$ meV. The energy difference between $\theta = 0$ and $\pi/2$ is about 50 meV, indicating a giant magnetic anisotropy.

The physics is shown in Fig. 6(b). The tetragonal ligand field on Co($3d$) orbitals brings about a partially occupied two-fold degenerate state dominated by d_{xz} and

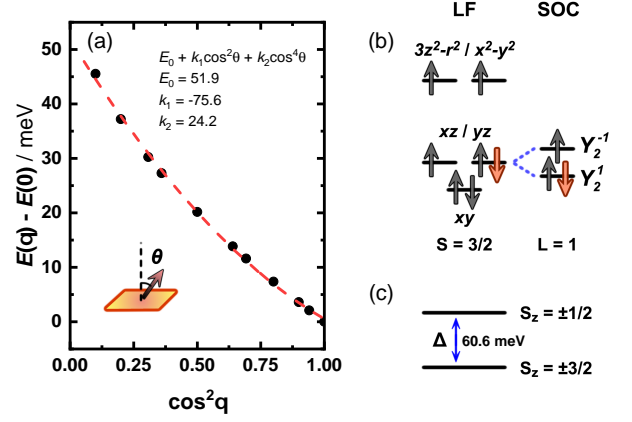


Figure 6. In DTC, (a) the relative total energy as a function of spin angle $\cos^2 \theta$; (b) under tetragonal ligand field (LF) and SOC, the schematic of electrons in Co($3d$) orbitals which bring about $S = 3/2, L = 1$ state; (c) the energy gap Δ between $S_z = \pm 3/2$ and $S_z = \pm 1/2$.

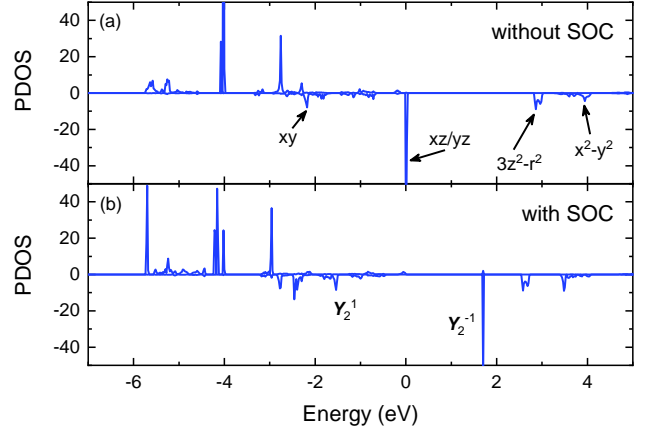


Figure 7. PDOS of Co($3d$) orbitals in DTC (a) without SOC and (b) with SOC. Positive and negative values corresponds to the spin-majority and spin-minority channels, respectively. The Fermi energy is set to zero.

d_{yz} orbitals. Due to the SOC, the degenerated d_{xz} and d_{yz} split into the spherical harmonics Y_2^1 and Y_2^{-1} . The fully filled Y_2^1 and the half filled Y_2^{-1} provide the orbital state $L_z = 1, L = 1$. The large orbital momentum along c axis pins the spin to the same direction by $L \cdot S$ and the energy scale of magnetic anisotropy is $\lambda = 21$ meV for Co, the coefficient of SOC, provides the energy scale of magnetic anisotropy.

According to projected density-of-state (PDOS) results of Co($3d$) orbitals, without SOC, the degenerate d_{xz} and d_{yz} orbitals have a sharp peak at spin-minority channel crossing the Fermi level. Then SOC lift this degeneracy and open a gap, consisting with the physics picture. DFT results also show that the orbital moment on Co is 1.46

μ_B which is even larger than $1.00 \mu_B$ by $L_z = 1$. It indicates the hybridization between d_{xy} and d_{xz}/d_{yz} .

Note that the coefficient k_2 , the fourth power term is considerable while for a $S = 3/2$ system only the quadratic term S_z^2 is allowed for the uniaxial magnetic anisotropy. It is because that the spins with local magnetic moment on Co in DFT calculations is regarded as a classical vector instead of a quantum spin state. To obtain the coefficient Δ of the zero field splitting $-\Delta S_z^2$, we converted each classical local magnetic moment state α to the superposition of the quantum spin eigenstates $|m\rangle$ by $|\alpha\rangle = \sum_{m=-3/2}^{3/2} c_m |m\rangle$. Then equation for that that spin configuration is:

$$E_\alpha = E_0 - \Delta \langle \alpha | \hat{S}_z^2 | \alpha \rangle \quad (6)$$

where E_α is the total energy for that spin configuration and E_0 is the spin-irrelevant energy. By solving the linear equations, we evaluated $\Delta = 60.6$ meV. Δ is also the energy gap Δ between two quantum spin states $S_z = \pm 1/2$ and $S_z = \pm 3/2$ (Fig. 6(c)). Since Δ is much large than J_c as well as the energy scale of thermal fluctuation, the spin states on DTC's Co always lay in $S_z = \pm 3/2$.

The shortcoming of DTC is that the system is not a covalently bonded spin chain although the anisotropy is huge. However, it can be used as a guidance for future synthesis.

B. DFT results on $\text{CoNa}(\text{N}_3)_2(\mathbf{L})$

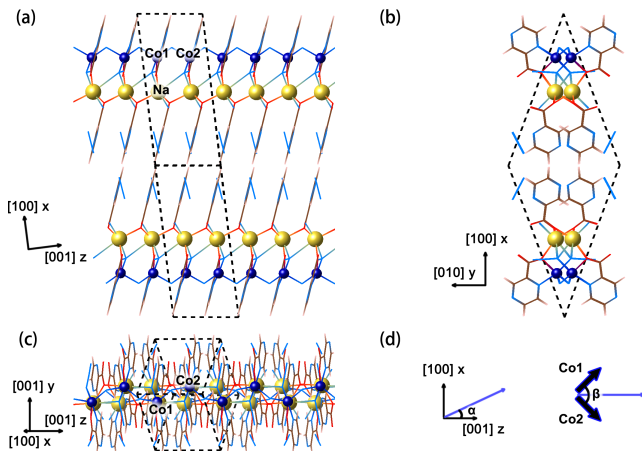


Figure 8. (a)-(c) three views of the structure of crystalline $\text{CoNa}(\text{N}_3)_2(\mathbf{L})$. Two Co atoms, Co1 and Co2, are labeled in the unit cell. (d) α is the angle between the total spin direction and $[001]$ direction and β is the angle between \mathbf{S}_1 and \mathbf{S}_2 , the spins on Co1 and Co2 respectively, representing the non-collinear spins.

Co-azido compounds $\text{CoNa}(\text{N}_3)_2(\mathbf{L})$, ($\mathbf{L} = \text{Pyrazine-2-carboxylato}$) is also a single-chain magnet. [22] Its crystalline phase has a based-centered

Table II. In $\text{CoNa}(\text{N}_3)_2(\mathbf{L})$, the total energy results for all collinear spin-configurations, including ΔE_{AF-FM} , the energy difference between ferromagnetic (FM) and antiferromagnetic (AF) spin configurations per Co-Co bonds, and the total energies relative to $[102]$ (The direction with the lowest total energy) per Co. non-SOC refers to the results without SOC included.

	ΔE_{AF-FM} (meV)	$E - E_{[102]}$ (meV)
without SOC	4.640	-
[001]	4.879	0.287
[010]	4.873	0.118
[100]	4.900	0.635
[011]	4.879	0.197
[101]	4.897	0.017
[110]	4.869	0.408
[0 $\bar{1}$ 1]	4.880	0.196
[10 $\bar{1}$]	4.884	0.922
[1 $\bar{1}$ 0]	4.884	0.393
[111]	-	0.059
[$\bar{1}$ 11]	-	0.645
[1 $\bar{1}$ 1]	-	0.058
[11 $\bar{1}$]	-	0.647
[102]	-	0.000
[10 $\bar{2}$]	-	0.724
[201]	-	0.200
[20 $\bar{1}$]	-	0.937

monoclinic lattice with space group $C2/c$ (No. 15), shown in Fig. 8. Each chain has two Co atoms, labeled Co1 and Co2, in one unit cell.

We perform DFT calculations with and without spin-orbit coupling included to investigate the magnetic properties of $\text{CoNa}(\text{N}_3)_2(\mathbf{L})$. In the calculations, the ab -plane in Fig. 8 is set to the xy -plane so that $[001]$ or z direction has an angle 6.94° with the c -axis.

We first perform total energy calculations for collinear spin configurations on Co. The total energy results are shown in Table. II. Without spin-orbit coupling (SOC), the energy difference between ferromagnetic (FM) and antiferromagnetic (AF) spin configurations per Co-Co bonds ΔE_{AF-FM} is 4.64 meV, indicating the FM coupling. When SOC is included, ΔE_{AF-FM} is 4.88 meV, almost invariant with spin directions, indicating that the anisotropic exchange interaction is ignorable. Therefore, the magnitude of exchange parameter J is $\Delta E_{AF-FM}/2S_1S_2 = 1.08$ meV (using broken-symmetry method: $J = \Delta E_{AF-FM}/(2S_1S_2 + S_{1(2)}) = 0.81$ meV), where $S_1 = S_2 = 3/2$ is the spin of Co1 and Co2 respectively.

The two neighboring Co atoms in one chain have the same magnitude and direction of magnetic anisotropy along the x and z directions, but they have opposite sign in magnetic anisotropy along the y direction. To determine the magnitude and direction of magnetic anisotropy, we selected the total energy results for collinear FM spin configurations in xz -plane, as a function of α , the angle between total magnetization and

[001] direction, shown in Fig. 9(a). The energy minimum is at $\alpha = 1.87\pi$ and the maximum energy difference is 0.92 meV.

Then we set non-collinear spin configurations where the total spins $\mathbf{S}_1 + \mathbf{S}_2$ is along $\alpha = 1.48\pi$ and the angle between \mathbf{S}_1 and \mathbf{S}_2 is β . The contribution of exchange interaction $-J\mathbf{S}_1 \cdot \mathbf{S}_2$ is subtracted from the total energies and the results are shown in Fig. 9(b). The energy minima are at $\beta = -0.30\pi$ and 1.70π and the maximum energy difference is 0.68 meV. Considering the on-site anisotropy Hamiltonian $\mathcal{H}_{aniso} = -D\tilde{S}_z^2 + E(\tilde{S}_x^2 - \tilde{S}_y^2)$ where the direction of \tilde{S}_z is the easy axis, we can obtain the magnitude of D as 0.36 meV (quantum: 0.54 meV) and E as 0.05 meV (quantum: 0.07 meV).

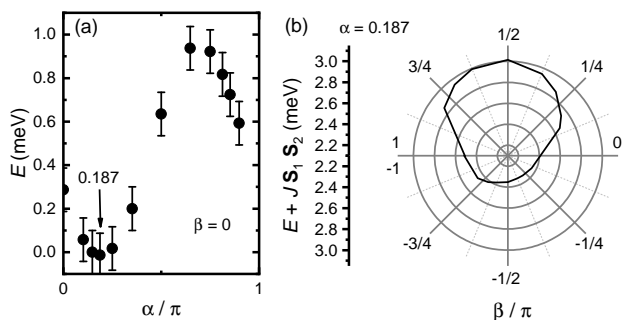


Figure 9. (a) The relative total energy E for collinear spin configurations ($\beta = 0$) as a function of total magnetization angle α . The error bar as $\pm 0.1\text{meV}$ refers to the precision of DFT. (b) The energy $E + J\mathbf{S}_1 \cdot \mathbf{S}_2$ ($J = 1.08$ meV) for non-collinear spin alignments as a function of non-collinear angle β . The magnetization angle α is fixed at 0.187π .

C. $\text{Co}(\text{NCS})_2(\text{thiourea})_2$

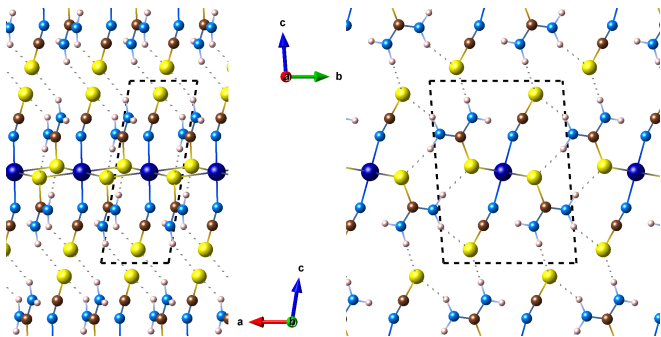


Figure 10. The structure of crystalline $\text{Co}(\text{NCS})_2(\text{thiourea})_2$. Dotted S–H bonds are H-bonds.

$\text{Co}(\text{NCS})_2(\text{thiourea})_2$ (thiourea = $\text{SC}(\text{NH}_2)_2$) is a new synthesised single-chain magnet (SCM) [23]. It is a Co-centered SCM where each Co atom with $S = 3/2$

high-spin state is surrounded by four in-plane S atoms of ligands thiourea and two out-of-plane N atoms of ligands NCS so that each Co is in a octahedral ligand-field, shown in Fig.10. Its crystalline phase has a triclinic lattice with space group $\text{P}\bar{1}$ so that it only has a inversion center on the centered Co atom.

According to the experiment, the intra-chain Co-Co spin exchange interaction is ferromagnetic coupling with $J \sim 0.31$ meV (3.63 K) and the inter-chain exchange interaction is very weak antiferromagnetic coupling with $J' \sim -0.027$ meV (-0.31 K). Each Co has a very strong uniaxial magnetic anisotropy with $D \sim 8.6$ meV (100 K) along N–Co–N direction. Our preliminary DFT results do not match with the experimental findings. Further DFT calculations are on-going.

III. ISING MODEL

The conventional starting point is the N site spin chain with Ising axis along the x direction in a transverse magnetic field,

$$H = -J \sum_{i=1}^{N-1} \sigma_i^x \sigma_{i+1}^x - h \sum_{i=1}^N \sigma_i^z, \quad (7)$$

where σ_i^x (σ_i^z) rotates spin i about the x (y) axis. J is the exchange strength and h is the magnitude of the magnetic field. When $h > J$ the system is paramagnetic with all spins pointing along the direction of the magnetic field. When $h < J$, the system is a degenerate ferromagnet. In particular, when the magnetic field is zero, the degenerate ground states are the configurations of the spins uniformly pointing parallel or uniformly pointing antiparallel to the Ising axis.

Using these spin operators one can construct a Jordan-Wigner (spinless) fermion at each site according to $c_j = (\sigma_j^x - i\sigma_j^y) [\prod_{l < j} (-\sigma_l^z)] / 2$. Inserting this definition into Eq. (7), the fermionic system is described by

$$H = -J \sum_{i=1}^{N-1} (c_i^\dagger c_{i+1} + c_i^\dagger c_{i+1}^\dagger + \text{H.c.}) - 2h \sum_{i=1}^N (c_i^\dagger c_i - 1/2). \quad (8)$$

which is simply the Kitaev model with nearest neighbor hopping and superconducting pairing J , chemical potential $2h$. In fermionic description, the system is topological trivial when $h > J$ and topologically nontrivially when $h < J$. According to the bulk-edge correspondence, this implies that in the latter case, there exists localized MBSs at the ends. In the Ising case, these take particularly simple forms in terms of the spin operators, $\gamma' = \sigma_1^x$ and $\gamma = -i\sigma_N^x \prod_N (-\sigma_l^z)$. These can be formed into a fermionic operator, $f = \sigma_1^x + \sigma_N^x \prod_N (-\sigma_l^z) / \sqrt{2}$, which also commutes with the Hamiltonian. Thus, the ground states can be

characterized by the occupancy of this fermion, $|1\rangle = (|\uparrow\rangle + |\downarrow\rangle)/\sqrt{2}$ and $|0\rangle = (|\uparrow\rangle - |\downarrow\rangle)/\sqrt{2}$.

Since the EPR will ultimately describe the transitions between energy levels, let us take a closer look at spectra in both the magnetic and fermionic pictures. Finding the eigenvalues of Eq. (7) gives the energies of all the states in the system, E_n . Because Eq. (8) is quadratic in the fermionic creation and annihilation operators, we can write it as a tight-binding model. Thus, the spectrum in the fermionic picture describes the set of levels, \mathcal{E}_n that can be occupied or unoccupied and the sum of the occupied levels describes the total energy of the system. Excited states are created by moving an occupied state to an unoccupied state; this is stipulated by the fact that states with energy below the chemical potential (hole states) must be moved to their particle conjugate.

We wish to subject our spin chain to a transverse oscillating magnetic field described by,

$$H_{\text{EPR}}(t) = \cos(\Omega t) \sum_{i=1}^N \sigma_i^z \sim \cos(\Omega t) \sum_{i=1}^N c_i^\dagger c_i. \quad (9)$$

The linear response of the system in the spin language is [30, 31]

$$G(\Omega) \sim \int dt \cos(\Omega t) \left\langle \left\{ \sum_{i=1}^N \sigma_i^z, \sum_{i=1}^N \sigma_i^z(t) \right\} \right\rangle, \quad (10)$$

where the expectation is with respect to one of the ground states and $\sigma_z(t)$ evolves according to Eq (7). For the spin system, this is straightforward to calculate numerically as we can directly evaluate the integrand for a sufficiently small system and, upon integration, we pick out the states with phase Ωt .

In the fermionic language we require a bit more massaging before we can numerically compute the EPR response. First, note that $\sigma_i^z = 2c_i^\dagger c_i - 1 = c_i^\dagger c_i - c_i c_i^\dagger$. For superconducting Hamiltonians, it is typical to use the Nambu doubling procedure in which we define a vector $\vec{c}_i = (c_i, c_i^\dagger)$. Notice that this makes Eq. (8) easy to handle in a single particle formalism. Also, $\sigma_i^z = \vec{c}_i^\dagger \tau^z \vec{c}_i$ with τ^z the Pauli z matrix acting in Nambu space. Let me now write yet another vector $\vec{C} = (c_1, c_1^\dagger, \dots, c_N, c_N^\dagger)$ which is $2N$ -dimensional. The total spin along the z axis can then be written as $\vec{C}^\dagger (\mathbb{I}_{N \times N} \otimes \tau^z) \vec{C} = \sum_{\alpha, \beta=1}^{2N} C_\alpha^\dagger (\tau^z)_{\alpha\beta} C_\beta$ where we have dropped the identity matrix. Let $\Lambda_{\nu\beta}$ be a matrix of the eigenvectors of Eq. (8) in rows so that the eigenoperators are $\vec{D} = \hat{\Lambda} \vec{C}$ or $D_\nu = \sum_\beta \Lambda_{\nu\beta} C_\beta$. Here, $[H, D_\nu] = \omega_\nu D_\nu$ and $D_\nu | \text{gnd} \rangle = 0$ if $E_\nu > 0$. Thus, the expression for the response in the fermionic language is

$$G(\Omega) \sim \int dt \cos(\Omega t) \sum \left[\left\langle D_{\mu'}^\dagger \Lambda_{\mu'\alpha'} \tau_{\alpha'\beta'}^z (\Lambda^\dagger)_{\beta'\nu'} D_{\nu'} e^{-i\omega_{\mu'} t} D_\mu^\dagger \Lambda_{\mu\alpha} \tau_{\alpha\beta}^z (\Lambda^\dagger)_{\beta\nu} D_\nu e^{-i\omega_\nu t} \right\rangle + \text{H.c.} \right], \quad (11)$$

where the summation is over repeated indices. Let us focus on the expectation value.

$$\begin{aligned} & \sum \left\langle D_{\mu'}^\dagger \Lambda_{\mu'\alpha'} \tau_{\alpha'\beta'}^z (\Lambda^\dagger)_{\beta'\nu'} D_{\nu'} e^{-i\omega_{\mu'} t} D_\mu^\dagger \Lambda_{\mu\alpha} \tau_{\alpha\beta}^z (\Lambda^\dagger)_{\beta\nu} D_\nu e^{-i\omega_\nu t} \right\rangle \\ &= \sum \left\langle \Lambda_{\mu'\alpha'} \tau_{\alpha'\beta'}^z (\Lambda^\dagger)_{\beta'\nu'} \Lambda_{\mu\alpha} \tau_{\alpha\beta}^z (\Lambda^\dagger)_{\beta\nu} \right\rangle e^{-i(\omega_{\mu'} - \omega_\nu)t} \left\langle D_{\mu'}^\dagger D_{\nu'} D_\mu^\dagger D_\nu \right\rangle \\ &= \sum \left\langle \Lambda_{\mu'\alpha'} \tau_{\alpha'\beta'}^z (\Lambda^\dagger)_{\beta'\nu'} \Lambda_{\mu\alpha} \tau_{\alpha\beta}^z (\Lambda^\dagger)_{\beta\nu} \right\rangle e^{-i(\omega_{\mu'} - \omega_\nu)t} (\langle D_{\mu'}^\dagger D_{\nu'} \rangle \langle D_\mu^\dagger D_\nu \rangle + \langle D_{\mu'}^\dagger D_\nu \rangle \langle D_{\nu'} D_\mu^\dagger \rangle) \\ &= \sum \left\langle \Lambda_{\mu'\alpha'} \tau_{\alpha'\beta'}^z (\Lambda^\dagger)_{\beta'\nu'} \Lambda_{\mu\alpha} \tau_{\alpha\beta}^z (\Lambda^\dagger)_{\beta\nu} \right\rangle e^{-i(\omega_{\mu'} - \omega_\nu)t} (\delta_{\mu'\nu'} \delta_{\mu\nu} \Theta(-E_{\mu'}) \Theta(-E_\nu) + \delta_{\mu'\nu} \delta_{\nu'\mu} \Theta(E_\mu) \Theta(-E_\nu)) \\ &= \sum \Theta(-E_{\mu'}) \Theta(-E_\mu) \Lambda_{\mu'\alpha'} \tau_{\alpha'\beta'}^z (\Lambda^\dagger)_{\beta'\nu'} \Lambda_{\mu\alpha} \tau_{\alpha\beta}^z (\Lambda^\dagger)_{\beta\nu} + e^{-i(\omega_{\mu'} - \omega_\nu)t} \Theta(E_\mu) \Theta(-E_{\mu'}) \Lambda_{\mu'\alpha'} \tau_{\alpha'\beta'}^z (\Lambda^\dagger)_{\beta'\mu} \Lambda_{\mu\alpha} \tau_{\alpha\beta}^z (\Lambda^\dagger)_{\beta\mu'}, \end{aligned}$$

where the Heaviside theta function is due to the occupancy (vacancy) of the states below (above) the Fermi energy. This quantity can be readily evaluated thus the response calculated. From the form of these expressions, the second term excites a filled state to a higher energy state then returns the system to the ground state. The first term is just the square of expectation value of the magnetization.

Although the magnetic case allows us to treat a more general system, i.e. when the effective fermion parity is not conserved, the fermionic language allows us to

treat a considerably larger chain as the dimension of the Hamiltonian in the magnetic and fermionic pictures is 2^N and $2N$, respectively. As we have checked to ensure both pictures result in identical EPR response, we present the results using the fermionic picture unless otherwise specified.

At this point we remark that the spin system is inversion symmetric, i.e. $i \rightarrow N - i + 1$. That is, in the fermion language, the inversion operator is $\hat{\mathcal{I}} = \sum_{j=1}^N c_j^\dagger c_{N-j-1}$ and $[\hat{\mathcal{I}}, H] = 0$. Moreover, because $\hat{\mathcal{I}}^2 = \mathbb{I}$, the eigenvectors of the Hamiltonian are also

eigenvectors of $\hat{\mathcal{L}}$ with eigenvalues of ± 1 . Lastly we note that $\hat{\mathcal{O}} = \sum_{j=1}^N c_j^\dagger c_j$ commutes with $\hat{\mathcal{L}}$. In first quantized language the latter is simply $\tau_{\alpha\beta}^z$ and $\Lambda_{\mu\alpha}\tau_{\alpha\beta}^z(\Lambda^\dagger)_{\beta\mu'}$ is matrix element of $\hat{\mathcal{O}}$ with respect to the eigenvectors μ and μ' . However, because $\hat{\mathcal{O}}$ cannot mix eigenvectors with different eigenvalues of $\hat{\mathcal{L}}$, EPR can only excite any filled state to half (rounded down) of the excited particle states. This will be important one analyzing the EPR spectra.

We calculate the EPR spectrum of a three-site chain in zero magnetic field with respect to both ground states (Fig. 11). The low energy peak corresponds to exciting the zero energy state to an excited state while the high energy peak corresponds to exciting quasiparticle hole. Because the quasiparticle energies are degenerate, there is no difference in the spectra between the ground states. In finite magnetic field, the band is no longer flat. Moreover, because the zero energy states have opposite eigenvalues of the operator $\hat{\mathcal{L}}$, the EPR spectrum of the ground states is different (Fig 12).

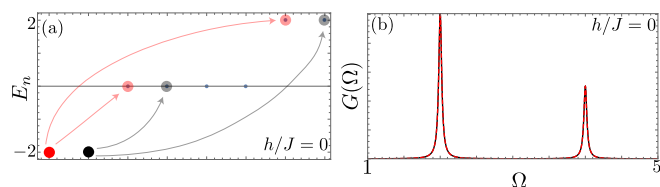


Figure 11. Spectrum indicating the transitions (a) that result in the EPR signal as a function of ac-magnetic field frequency, Ω (b), with $h = 0$.

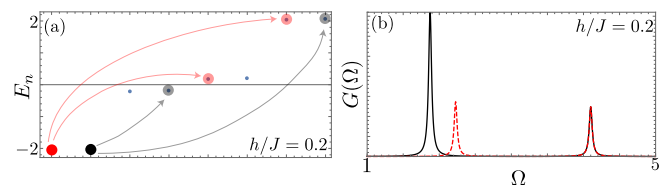


Figure 12. Spectrum indicating the transitions (a) that result in the EPR signal as a function of ac-magnetic field frequency, Ω (b), with $h/J = 0.2$.

* Correspond to: hping@ufl.edu

[1] M. Böhme and W. Plass, *Chemical Science* **10**, 9189 (2019).
 [2] J. M. Zadrozny and J. R. Long, *Journal of the American Chemical Society* **133**, 20732 (2011).
 [3] R. Boca, H. Elias, W. Haase, M. Hüber, R. Klement, L. Müller, H. Paulus, I. Svoboda, and M. Valko, *Inorganica Chimica Acta* **278**, 127 (1998).
 [4] R. Boča, L. Dlháň, W. Haase, R. Herchel, A. Mašlejová, and B. Papánková, *Chemical Physics Letters* **373**, 402 (2003).

[5] F. Neese, *WIREs Computational Molecular Science* **2**, 73 (2012).
 [6] F. Neese, *WIREs Computational Molecular Science* **8** (2017).
 [7] C. Angeli, R. Cimraglia, S. Evangelisti, T. Leininger, and J. P. Malrieu, *The Journal of Chemical Physics* **114**, 10252 (2001).
 [8] C. Angeli, R. Cimraglia, and J.-P. Malrieu, *Chemical Physics Letters* **350**, 297 (2001).
 [9] C. Angeli, R. Cimraglia, and J.-P. Malrieu, *The Journal of Chemical Physics* **117**, 9138 (2002).
 [10] D. A. Pantazis, X.-Y. Chen, C. R. Landis, and F. Neese, *Journal of Chemical Theory and Computation* **4**, 908 (2008).
 [11] F. Weigend and R. Ahlrichs, *Physical Chemistry Chemical Physics* **7**, 3297 (2005).
 [12] J. P. Perdew, *Physical Review B* **33**, 8822 (1986).
 [13] A. D. Becke, *Physical Review A* **38**, 3098 (1988).
 [14] A. D. Becke, *The Journal of Chemical Physics* **98**, 5648 (1993).
 [15] F. Neese, *Journal of Computational Chemistry* **24**, 1740 (2003).
 [16] F. Neese, F. Wennmohs, A. Hansen, and U. Becker, *Chemical Physics* **356**, 98 (2009).
 [17] S. Kossmann and F. Neese, *Chemical Physics Letters* **481**, 240 (2009).
 [18] S. Kossmann and F. Neese, *Journal of Chemical Theory and Computation* **6**, 2325 (2010).
 [19] R. Izsák and F. Neese, *The Journal of Chemical Physics* **135** (2011).
 [20] R. Izsák and F. Neese, *Molecular Physics* **111**, 1190 (2013).
 [21] E. A. Sutturina, D. Maganas, E. Bill, M. Atanasov, and F. Neese, *Inorganic Chemistry* **54**, 9948 (2015).
 [22] B.-W. Hu, J.-P. Zhao, Q. Yang, X.-F. Zhang, M. Evangelisti, E. C. Sañudo, and X.-H. Bu, *Dalton Transactions* **39**, 11210 (2010).
 [23] S. P. M. Curley, R. Scatena, R. C. Williams, P. A. Goddard, P. Macchi, T. J. Hicken, T. Lancaster, F. Xiao, S. J. Blundell, V. Zapf, J. C. Eckert, E. H. Krenkel, J. A. Villa, M. L. Rhodehouse, and J. L. Manson, *Phys. Rev. Materials* **5**, 034401 (2021).
 [24] A. Lopez-Castro and M. R. Truter, *J. Chem. Soc. NA*, 1309 (1963).
 [25] V. S. Zapf, V. F. Correa, P. Sengupta, C. D. Batista, M. Tsukamoto, N. Kawashima, P. Egan, C. Pantea, A. Migliori, J. B. Betts, M. Jaime, and A. Paduan-Filho, *Phys. Rev. B* **77**, 020404 (2008).
 [26] M. Yazback, J.-X. Yu, S. Liu, L. Zhang, N. S. Sullivan, and H.-P. Cheng, *Phys. Rev. B* **103**, 054434 (2021).
 [27] C.-C. Ni and H. Weinstock, *Physics Letters A* **34**, 3 (1971).
 [28] E. Ruiz, J. Cano, S. Alvarez, and P. Alemany, *Journal of Computational Chemistry* **20**, 1391 (1999).
 [29] E. Ruiz, A. Rodríguez-Forteza, J. Cano, S. Alvarez, and P. Alemany, *Journal of Computational Chemistry* **24**, 982 (2003).
 [30] G. O. Berim and A. R. Kessel, *Physica B+C* **96**, 71 (1979).
 [31] R. Kubo and K. Tomita, *Journal of the Physical Society of Japan* **9**, 888 (1954).